**Showcasing research from Professor Jerry Chun Chung Chan's laboratory, Department of Chemistry, National Taiwan University, Taipei, Taiwan.**

Site specific NMR characterization of abeta-40 oligomers cross seeded by abeta-42 oligomers

By exploiting the spatial-confinement and the material-exchange features of reverse micelles, we are able to prepare the oligomeric aggregates of beta amyloid peptides which are uniform in size and structurally monomorphic. Our protocol not only allows an active control of the size of the oligomers, but also provides a versatile approach for the study of the protein–protein interactions associated with amyloidogenic peptides.

## As featured in:


See Jerry Chun Chung Chan *et al.*, *Chem. Sci.*, 2022, **13**, 8526.

ROYAL SOCIETY OF CHEMISTRY

rsc.li/chemical-science

Registered charity number: 207890

Chemical Science

ROYAL SOCIETY OF CHEMISTRY

EDGE ARTICLE

View Article Online
View Journal | View Issue



Cite this: *Chem. Sci.*, 2022, **13**, 8526

All publication charges for this article have been paid for by the Royal Society of Chemistry

# Site specific NMR characterization of abeta-40 oligomers cross seeded by abeta-42 oligomers†

Han-Wen Chang,[a] Ho-I. Ma,[a] Yi-Shan Wu,[a] Ming-Che Lee,[a] Eric Chung-Yueh Yuan,[a] Shing-Jong Huang,[b] Yu-Sheng Cheng,[a] Meng-Hsin Wu,[c] Ling-Hsien Tu[c] and Jerry Chun Chung Chan *[a]

Received 17th March 2022
Accepted 12th June 2022

DOI: 10.1039/d2sc01555b

rsc.li/chemical-science

Extracellular accumulation of β amyloid peptides of 40 ($A\beta_{40}$) and 42 residues ($A\beta_{42}$) has been considered as one of the hallmarks in the pathology of Alzheimer's disease. In this work, we are able to prepare oligomeric aggregates of Aβ with uniform size and monomorphic structure. Our experimental design is to incubate Aβ peptides in reverse micelles (RMs) so that the peptides could aggregate only through a single nucleation process and the size of the oligomers is confined by the physical dimension of the reverse micelles. The hence obtained Aβ oligomers (AβOs) are 23 nm in diameter and they belong to the category of high molecular-weight (MW) oligomers. The solid-state NMR data revealed that $A\beta_{40}$Os adopt the structural motif of β-loop-β but the chemical shifts manifested that they may be structurally different from low-MW AβOs and mature fibrils. From the thioflavin-T results, we found that high-MW $A\beta_{42}$Os can accelerate the fibrillization of $A\beta_{40}$ monomers. Our protocol allows performing cross-seeding experiments among oligomeric species. By comparing the chemical shifts of $A\beta_{40}$Os cross seeded by $A\beta_{42}$Os and those of $A\beta_{40}$Os prepared in the absence of $A\beta_{42}$Os, we observed that the chemical states of E11, K16, and E22 were altered, whereas the backbone conformation of the β-sheet region near the C-terminus was structurally invariant. The use of reverse micelles allows hitherto the most detailed characterization of the structural variability of $A\beta_{40}$Os.

## Introduction

Aggregation of amyloid beta peptides (Aβ) is closely associated with Alzheimer's disease (AD), where the 40-residue ($A\beta_{40}$) and 42-residue ($A\beta_{42}$) peptides are two major Aβ species derived from amyloid precursor protein (APP).[1–3] Their primary sequences are identical from residues 1–40 and the two additional residues at the C-terminus of $A\beta_{42}$ are I41 and A42. Although the severity of dementia correlates only weakly to the density or number of fibrillar amyloid plaques, there is a robust correlation between soluble Aβ levels and the extent of synaptic loss.[4–6] Since the discovery of Aβ oligomers (AβOs) as potent neurotoxins,[7] it is increasingly accepted that AβOs are the most pathogenic form of Aβ.[8–11] There is a continuous distribution of soluble Aβ species from monomeric form up to oligomers in excess of 100 kDa.[5] At the molecular level, a chemical equilibrium is being re-established among the large with smaller species and monomers. Therefore, it is very difficult to obtain a homogeneous preparation of a particular oligomeric species,[9] rendering the comparison of the biochemical results of AβOs in the literature very difficult.[12] Oligomers of low molecular weight (low-MW) refer to AβOs of MW ≤ 30 kDa, whereas high-MW AβOs have MW > 100 kDa.[5] There are many different ways to prepare low-MW AβOs.[13] Dimers of Aβ peptides can be prepared by the use chemical linkers.[14–16] The technique of photo induced cross-linking of unmodified proteins has been used to demonstrate that the $A\beta_{40}$ tetramers ($n = 4$) and other low-$n$ are in rapid equilibrium, whereas the stable oligomers of $A\beta_{42}$ ($n = 5$ and 6) have a strong propensity to assemble further to form super-structures.[17–19] Very recently, homogenous and stable $A\beta_{42}$ tetramers and octamers were successfully prepared in detergent micelles.[20,21] On the other hand, high-MW AβOs are usually prepared by incubating the monomer solution of Aβ *in vitro* at relatively low temperature or in a short period of time.[22–28] Other chemical approaches such as binding with metal ions,[29,30] antibody,[31] small molecules,[32,33] and polymer-nanodiscs[34] have also been developed to prepare high-MW AβOs. Both the low-MW and high-MW Aβ aggregates have different impacts on synapses.[10] In fact, high-MW AβOs may dissociate into low-MW AβOs in mildly alkaline aqueous buffer.[35] Currently, it remains unsettled which forms of AβOs are the true culprits of AD.[6,11]

[a]*Department of Chemistry, National Taiwan University, No. 1, Section 4, Roosevelt Road, Taipei, 10617, Taiwan. E-mail: chanjcc@ntu.edu.tw*

[b]*Instrumentation Center, National Taiwan University, No. 1, Section 4, Roosevelt Road, Taipei, 10617, Taiwan*

[c]*Department of Chemistry, National Taiwan Normal University, No. 88, Section 4, Ting-Chow Road, Taipei, 11677, Taiwan*

† Electronic supplementary information (ESI) available. See https://doi.org/10.1039/d2sc01555b

The aggregation of $A\beta_{40}$ and $A\beta_{42}$ have different dependence on the peptide concentration or other environmental factors.[36] The kinetic profiles of the Aβ aggregation process usually comprise the lag phase, elongation, and eventually the plateau phase. Adding fragments of preformed fibrils (fibril seeds) of the same protein can significantly shorten the period of lag phase. This phenomenon, known as self-seeding, is consistent with the nucleation-growth mechanism.[37,38] While the self-seeding effect has been well established for $A\beta_{40}$ and $A\beta_{42}$,[39–43] the situation is more complicated for the cross seeding between $A\beta_{40}$ and $A\beta_{42}$. Earlier reports suggested that the aggregation of $A\beta_{40}$ monomers can be facilitated by the presence of $A\beta_{42}$ fibril seeds.[40,42,44] By contrast, more recent studies reported that the seeding effect of $A\beta_{42}$ fibrillar seeds on $A\beta_{40}$ monomer is insignificant.[45,46] Indeed, solid-state NMR studies revealed that the backbone conformation of the β-strands of $A\beta_{40}$ and $A\beta_{42}$ fibrils are different.[47–49] The formation of a sufficiently large peptide cluster, which is coined as the "nucleus" according to the classical nucleation theory for crystal growth, is the most critical event of Aβ aggregation. As proposed by Knowles and co-workers,[50–53] the formation of Aβ nucleus can occur *via* the processes of primary nucleation, fibril fragmentation, and the fibril-assisted mechanism (secondary nucleation). The existence of multiple nucleation pathways might well be the underlying physical reason for the structural polymorphism commonly observed for Aβ aggregates prepared in bulk solution.[54] Furthermore, it has been argued that the interaction between $A\beta_{40}$ and $A\beta_{42}$ was restricted at the step of primary nucleation.[45] The aforementioned studies indicated that it is highly desirable to develop a method to control the aggregation pathway of Aβ peptides so that the interaction between $A\beta_{40}$ and $A\beta_{42}$ could be characterized at the molecular level.

Reverse micelles (RMs), which correspond to water droplets in an oil phase, have been extensively used as microreactors for a large variety of materials.[55,56] In this chemical system, the RMs undergo coalescence and separation at a rate constant of $10^6$–$10^8$ $dm^3\ mol^{-1}\ s^{-1}$.[57] The material transfer among RMs has been convincingly demonstrated in many studies of enzymatic activities, where substrate molecules were delivered to the enzyme *via* the continuous fusion and fission of RMs.[55,58,59] Consequently, we hypothesize that Aβ peptides could aggregate *via* a single nucleation process in a space confined by the physical dimension of RMs. This concept has been proved feasible in our earlier attempt to prepare protofibrils (curvilinear fibrils) of $A\beta_{40}$ peptides.[60] In this work, we have prepared high-MW oligomeric aggregates of $A\beta_{40}$ with a single dominant structure (monomorphic) based on the RMs formed by the non-ionic surfactants poly(oxyethylene) nonylphenyl ether (Igepal CO520). For the first time in the literature, we were able to prepare $A\beta_{40}$Os cross seeded by $A\beta_{42}$Os. The solid-state NMR results showed that the chemical states of E11, K16, and E22 of $A\beta_{40}$ are altered upon the interaction between high-MW $A\beta_{42}$Os and $A\beta_{40}$ peptides.

# Results

### Molecular weight of $RM_{CO520}A\beta_{40}$

The purity of the Aβ peptides were >95% (Fig. S1†). Size exclusion chromatography (SEC) and dynamic light scattering (DLS) were used to confirm that the freshly prepared $A\beta_{40}$ peptides were in monomeric state (Fig. S2 and S3†). $A\beta_{40}$ monomers (100 μM) were incubated in the RMs formed by the ternary system of CO520/cyclohexane/$NH_4OAc_{(aq)}$ for 7 d (Fig. S4†).[61] DLS measurements indicated that the RMs were stable for at least 10 days (Fig. S5†), where the RMs had a size of *ca.* 23 nm with polydispersity index (PdI) less than 0.10. To back extract the Aβ peptides from the RM solution, the stripping buffer ($ZnCl_2$, 50 μM) was added to the RM solution. The $ZnCl_2$ solution was used to suppress any further aggregation of the AβOs.[62] The aqueous phase was then lyophilized to remove ammonium acetate and water. The obtained powder sample is henceforth referred to as $RM_{CO520}A\beta_{40}$. To estimate the amount of residual CO520, we carried out elemental analysis (EA) for $RM_{CO520}A\beta_{40}$ (Fig. S6 and Table S1†). CO520 and $A\beta_{40}$ had different contributions to the atomic percentage of C, N, S, H of $RM_{CO520}A\beta_{40}$. As shown in Fig. S6,† the molar ratio of CO520 to $A\beta_{40}$ was estimated to be $9.0 \pm 0.7$. In addition, the mass percentage of $A\beta_{40}$ was *ca.* 24.9%, from which the efficiency of the back extraction of Aβ peptides was calculated to be *ca.* 66%. Although analytical size exclusion chromatography (SEC) could be used to estimate the MW of protein aggregates, it has been pointed out that the results for AβOs are unreliable because of the possible interaction between Aβ peptides and the SEC column material.[28] On the other hand, the mass-per-length of amyloid fibrils can be accurately determined by scanning transmission microscopy (STEM) or tilted-beam TEM using tobacco mosaic virus (TMV) rods as reference objects.[63] Fig. 1 shows the STEM image of $RM_{CO520}A\beta_{40}$ and TMV, where the size of $RM_{CO520}A\beta_{40}$ particles was $23.1 \pm 5.3$ nm (Fig. S7†). Following the procedure described in the ESI,† the MW of $RM_{CO520}A\beta_{40}$, which contained CO520 and $A\beta_{40}$, was determined as 4600 kDa, from which the AβO in $RM_{CO520}A\beta_{40}$ was estimated to have an MW of 2400 kDa (~554 monomers). In comparison, the amyloid intermediate ($I_\beta$) of $A\beta_{40}$, with a size of 10–35 nm, was estimated to have MW ≥ 650 kDa by a glycerol gradient sedimentation assay.[23] Using a similar method, the patient derived amylospheroids (ASPDs, 10–15 nm) were reported to have MW in the range of 158–669 kDa.[64,65] It is well known that Aβ oligomers are poorly defined in size and a distribution of 150–1000 kDa has been reported for Aβ peptides in bulk solution by multiangle laser light scattering detection.[66] While $RM_{CO520}A\beta_{40}$ is a non-fibrillar aggregate of $A\beta_{40}$, its sizable MW suggested that $RM_{CO520}A\beta_{40}$ might possess the structural features required for the onset of fibrillar growth. We note in passing that micelle-like aggregates of $A\beta_{40}$ peptides of 7 nm in diameter were identified as the nucleation center for $A\beta_{40}$ fibrillization.[67,68]

### Seeding and self-aggregating effects of $RM_{CO520}A\beta$

The seeding effects of $RM_{CO520}A\beta_{40}$ on $A\beta_{40}$ monomers (25 μM) was examined by the thioflavin T (ThT) assay, where EDTA solution was added to chelate $Zn^{2+}$ ions. The control sample was prepared in the absence of Aβ peptides ($RM_{CO520}$). As expected, the seeding effect of $RM_{CO520}A\beta_{40}$ on $A\beta_{40}$ monomers was revealed by the shortening of the lag time (Fig. 2). Remarkably, the ThT results revealed that $RM_{CO520}A\beta_{42}$ was also able to

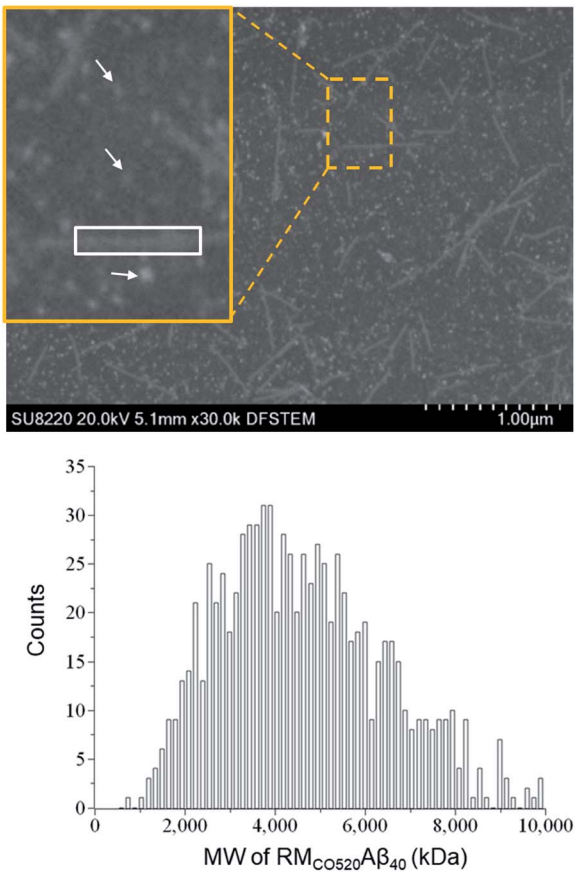


Fig. 1 STEM image of a mixture of $RM_{CO520}A\beta_{40}$ and TMV. Typical oligomers of $RM_{CO520}A\beta_{40}$ are indicated by arrows. The rectangular box in white shows a fragment of TMV. The mean value of the MW of $RM_{CO520}A\beta_{40}$ was estimated to be 4600 kDa, which was obtained by the bootstrapping resampling method.

promote the aggregation of $A\beta_{40}$ monomers. Recently, it has been demonstrated that the oligomeric aggregates of a chimeric peptide can completely eliminate the lag period of $A\beta_{40}$, resulting in immediate fibril elongation.[16] Although the lag phase of $A\beta_{40}$ was not completely eliminated by $RM_{CO520}A\beta_{42}$, the extent of the shortening of the lag period was comparable to what reported for the cross-seeding effect between $A\beta_{40}$ and $A\beta_{42}$.[69] Similar ThT results were observed when the amount of seeds was increased from 4% to 10% (Fig. S8†). Amyloid fibrils were also formed by the self-aggregation of $RM_{CO520}A\beta$ (Fig. S9†). Goto and co-workers reported that protein-detergent complex would become an off-pathway aggregate when the mixed micelles of detergent and protein are thermodynamically and kinetically more stable than the amyloid fibrils.[70] Because CO520 is a non-ionic surfactant (Fig. S4†), its interaction with Aβ peptides are expected to be small. The self-aggregating behaviors of $RM_{CO520}A\beta$ indicated that CO520 did not form any stable complex with Aβ peptides.

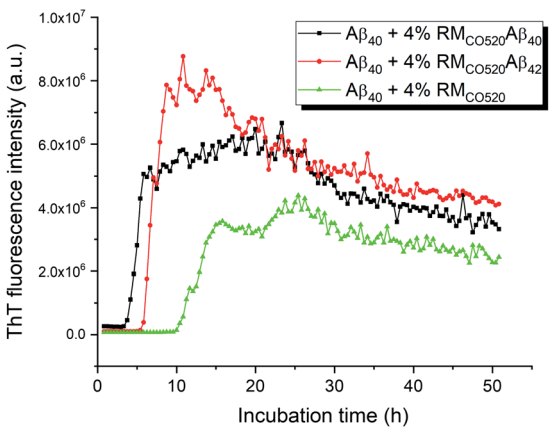


Fig. 2 ThT Fluorescence results for probing the seeding effects of $RM_{CO520}A\beta$. For all the measurements, the concentration of $A\beta_{40}$ monomer was 25 μM. The amount of the seeds was adjusted to 4 mole% of the monomers. $RM_{CO520}$ was prepared in the absence of Aβ peptides.

Interactions between Aβ alloforms could modulate their aggregation behaviors *in vitro*.[71] Previous studies suggested that there is a significant molecular cross-talk between $A\beta_{40}$ monomers and various aggregation states of $A\beta_{42}$.[40,42,44] In particular, $A\beta_{40}$ monomers have strong binding affinity for $A\beta_{42}$ aggregates.[72,73] Because the aggregation kinetics of $A\beta_{42}$ is much faster than $A\beta_{40}$,[53] we attempted to investigate the effect of $A\beta_{42}$Os on the aggregation process of $A\beta_{40}$ monomers through our RM system. Briefly, the $A\beta_{42}$ peptides were first incubated for three days and $A\beta_{40}$ monomers were subsequently added in such a way that the final molar ratio of $A\beta_{42}$ and $A\beta_{40}$ was 1 : 1. We henceforth refer the sample to as $RM_{CO520}A\beta_{42/40}$, which also exhibited seeding effects on $A\beta_{40}$ monomers and the self-aggregating behavior (Fig. S10 and S11†). The size of $RM_{CO520}$-$A\beta_{42/40}$ particles was 22.5 ± 6.1 nm (Fig. S12†), indicating that the size of both AβOs were constrained by the physical dimension of the RMs. The ThT fluorescence excitation spectrum revealed that ThT molecules can bind to $RM_{CO520}A\beta_{42/40}$, $RM_{CO520}A\beta_{42}$, and $RM_{CO520}A\beta_{40}$ (Fig. S13†), which verified that these high-MW Aβ oligomers had fibril-like structures.

## Structural motif of $RM_{CO520}A\beta_{40}$

Four $^{13}C$ enriched samples of $RM_{CO520}A\beta_{40}$ were prepared, covering 23 residues in the region from E11 to V40 (Table S2†). The enrichment level was 60%. A typical $^{13}C$–$^{13}C$ correlation spectrum acquired for $RM_{CO520}A\beta_{40}$ is shown in Fig. 3. While structural polymorphism was commonly observed for the $A\beta_{40}$Os or Aβ fibrils prepared in bulk solution,[26,54] the structure of $RM_{CO520}A\beta_{40}$ was monomorphic as evidenced by the fact that the NMR spectra were basically dominated by a single set of signals (Fig. S14–S16†). We attributed this favorable result to the scenario that the nucleation process of $A\beta_{40}$ in a reverse micelle (23 nm in diameter) was dominated by a single pathway. The TEM images of the samples after the solid-state NMR measurements confirmed that the samples remained in the oligomeric state (Fig. S17†). The full width at half maximum (FWHM) data, with an average of 3.4 ppm (Fig. 4), were larger than the fibrillar aggregates.[74] We did not rehydrate the lyophilized oligomer samples for NMR measurements, in order to prevent fibrillization from occurring. Although oligomeric aggregates of Aβ are transient species, the FWHM data

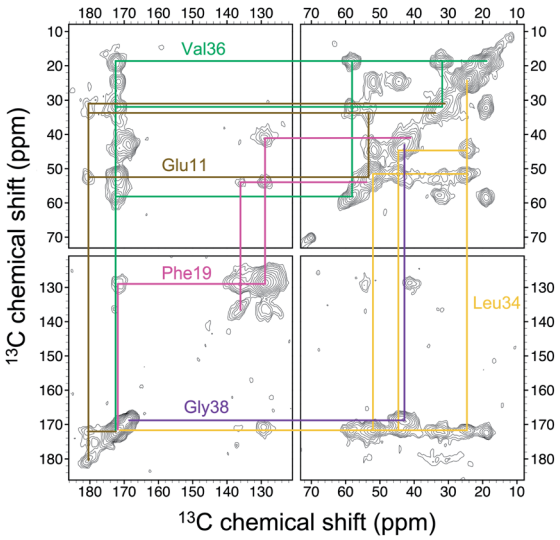


Fig. 3 Spectral assignment for the $^{13}$C homonuclear correlation spectrum of $RM_{CO520}A\beta_{40}$ with uniformly $^{13}$C and $^{15}$N labeling at E11, F19, L34, V36, and G38 (sample S1). The contour levels were increased by a factor of 1.4 successively, where the base levels were set to 4× root-mean-square noise.

supported that the molecular structure of $RM_{CO520}A\beta_{40}$ was not completely disordered. All the chemical shift data are summarized in Table S3,† from which the backbone torsion angles were estimated by TALOS-N.[75] Fig. S18† illustrates the backbone torsion angles, indicating that the structural motif adopted by $RM_{CO520}A\beta_{40}$ was $\beta_1$-loop-$\beta_2$, which is the same as that of the spherical amyloid assembly (SPA) of $A\beta_{42}$.[76] The similar structural motif for $A\beta_{40}$Os and $A\beta_{42}$Os is consistent with the observation that both $RM_{CO520}A\beta_{40}$ and $RM_{CO520}A\beta_{42}$ could seed the fibrillization of $A\beta_{40}$ monomers.

The chemical shift data revealed some interesting structural features of $RM_{CO520}A\beta_{40}$. The backbone chemical shifts of $RM_{CO520}A\beta_{40}$ were very different from those reported for $A\beta_{40}$ fibrils (Fig. 5), where $^{13}$C chemical shifts of mature fibrils were taken from wild-type $A\beta_{40}$ fibrils incubated under quiescent conditions and agitated conditions,[77] and brain-derived $A\beta_{40}$ fibrils.[78–80] The data for Aβ oligomers were taken from low-MW $A\beta_{40}$Os,[26] SPA,[76] ASPD,[27] and $I_\beta$.[23] Overall, a large chemical shift difference (>1.5 ppm) was found at the loop region (D23 to N27). Glycine residues are important structural markers for sharp loops or turns in amyloid structures because of their structural flexibility.[49,81] Accordingly, the FWHM of all the $^{13}$C enriched glycines of $RM_{CO520}A\beta_{40}$ were >4 ppm. Comparing the glycine chemical shifts of $RM_{CO520}A\beta_{40}$ and those reported for *in vitro* fibrillar aggregates of $A\beta_{40}$, a large discrepancy (>2 ppm) was observed at G25 and G33, whereas a reasonable agreement was at G38 (Fig. S19†). We surmised that a major conformational change between high-MW $A\beta_{40}$Os and $A\beta_{40}$ fibrils occurred at G25 and G33. While the structure of Aβ oligomers could be fibrillar like,[82] a recent solid-state NMR study suggested that there is a significant difference in supramolecular organization between protofibrils and fibrils.[28] Thus, it is possible that the supramolecular structure of $RM_{CO520}A\beta_{40}$ was different from mature fibrils. On the other hand, the backbone chemical shifts of $RM_{CO520}A\beta_{40}$, albeit very similar to those reported for $I_\beta$ (high-MW $A\beta_{40}$Os), exhibit a significant difference from those reported for low-MW $A\beta_{40}$Os (Fig. S20†).[26] In other words, there could be a continuous structural evolution from low-MW $A\beta_{40}$Os, to high-MW $A\beta_{40}$Os, and then to mature fibrils.[28] But

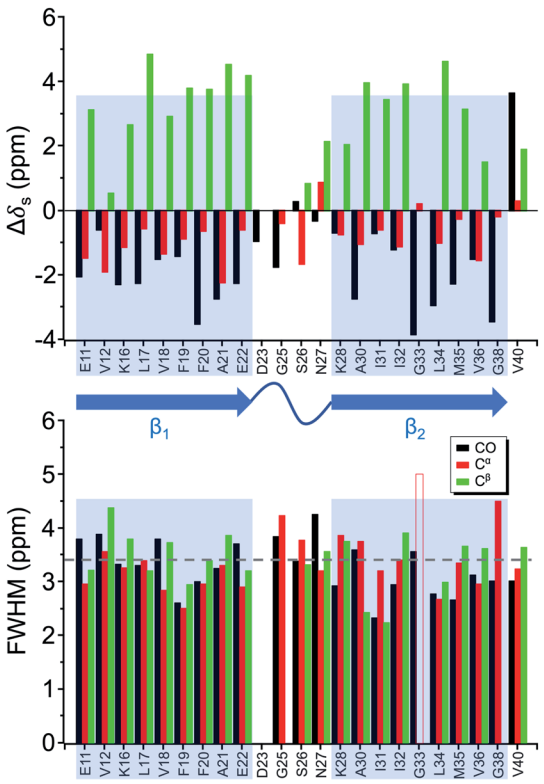


Fig. 4 Secondary chemical shift (upper trace) and full width at half maximum (FWHM) of the NMR signals (lower trace) extracted from the $^{13}$C–$^{13}$C correlation spectra of $RM_{CO520}A\beta_{40}$. The β-sheet region was highlighted in shaded rectangular blocks. The dashed line indicates the average FWHM. The open bar denotes FWHM > 5 ppm.

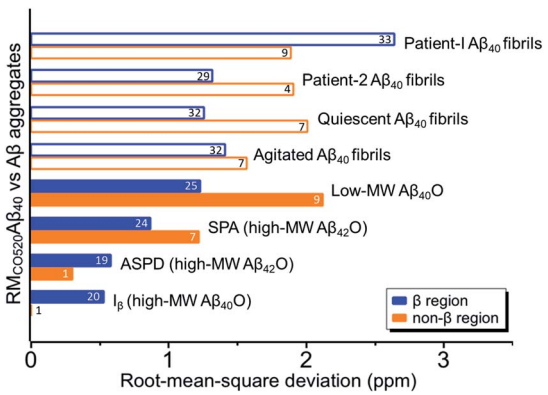


Fig. 5 Comparison of the $C^\alpha$ and $C^\beta$ chemical shifts of $RM_{CO520}A\beta_{40}$ and the data of other $A\beta_{40}$ aggregates in the literature. Solid bars indicate the results obtained for oligomeric species and open bars for fibrillar aggregates. The number of the data points for calculating the rms deviations are shown on the bars, which were largely limited by the availability of the literature data. The β-sheet and non-β-sheet regions were defined with respect to the $RM_{CO520}A\beta_{40}$ sample.

this hypothesis has to be validated by more experimental evidences. In fact, it is not yet clear whether such difference in chemical shift is owing to the difference in incubation conditions or the size effect of the oligomers. We also note that the long-range contact between F19 and L34 were not observed in this work. While the relatively low level of $^{13}C$ enrichment (60%) might have rendered the contact unobservable, it is equally plausible that such contact was absent in our samples.[83]

### Structural motif of oligomeric $RM_{CO520}A\beta_{42/40}$

In the foregoing section, we have demonstrated that RMs could be used to investigate the effect of $A\beta_{42}Os$ on the aggregation process of $A\beta_{40}$. We carried out solid-state NMR measurements of $RM_{CO520}A\beta_{42/40}$ with the same isotopic labeling scheme as $RM_{CO520}A\beta_{40}$ (Fig. S21–24 and Table S4†). To facilitate the comparison of the data of $RM_{CO520}A\beta_{40}$ and $RM_{CO520}A\beta_{42/40}$, only the $A\beta_{40}$ peptides were $^{13}C$ enriched for the latter. Fig. 6 shows the selected excerpts of the spectra of $RM_{CO520}A\beta_{40}$ and $RM_{CO520}A\beta_{42/40}$. In addition to $A\beta_{40}Os$ and $A\beta_{42}Os$, $RM_{CO520}$-$A\beta_{42/40}$ might, in principle, contain the oligomeric aggregates of a mixture of $A\beta_{40}$ and $A\beta_{42}$ because of the continuous attachment and detachment of Aβ peptides from AβOs. Were it the case that the $A\beta_{40}$ peptides of $RM_{CO520}A\beta_{42/40}$ had different local environments, multiple sets of NMR signals would have been observed for all the residues. Interestingly, the NMR spectra of $RM_{CO520}A\beta_{42/40}$ were again dominated by a single set of signals for the $\beta_2$ region, suggesting that $RM_{CO520}A\beta_{42/40}$ did not contain a random oligomeric mixture of $A\beta_{40}$ and $A\beta_{42}$. That is, $A\beta_{42}Os$ were relatively stable and would not dissociate during the aggregation of $A\beta_{40}$ peptides. Overall, the region of the $\beta_1$-loop-$\beta_2$ motif is the same for $RM_{CO520}A\beta_{40}$ and $RM_{CO520}A\beta_{42/40}$, as indicated by the secondary chemical shifts (Fig. S25†). With reference to the data shown in Fig. 7, we found that the backbone $^{13}C$ chemical shift difference between $RM_{CO520}A\beta_{42/40}$ and $RM_{CO520}A\beta_{40}$ was immaterial in the $\beta_2$ region (K28 to G38), where the only exception was A30-$C^{\alpha}$. Thus, it is legitimate to infer that their backbone conformations were largely the same. On the other hand, relatively large chemical shift deviations were observed for some residues, *viz.*, E11, K16, E22, G25, and S26. In addition, the FWHM data shown in Fig. S26† revealed that N27, K28, and G33 of $RM_{CO520}A\beta_{42/40}$ might have considerable difference in structural disorder and/or motional dynamics from $RM_{CO520}A\beta_{40}$. For other residues with minor chemical shift deviation, a careful scrutiny of the cross-peak patterns revealed that there were multiple cross peaks for the region of LVFFA (Fig. S27†). That is, the intermolecular packing of $A\beta_{40}$ peptides in that region was rather heterogeneous, but their backbone and sidechain conformations were largely the same.

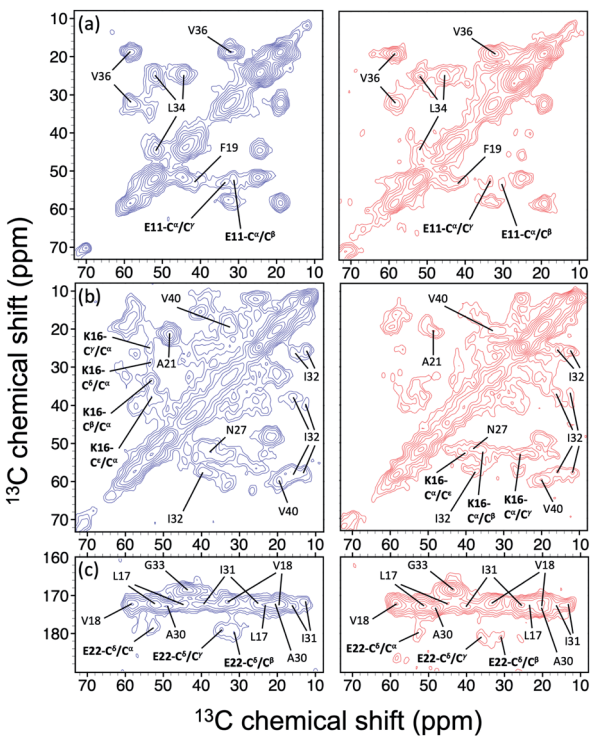


Fig. 6 Comparison of the excerpts of the $^{13}C$–$^{13}C$ correlation spectra of $RM_{CO520}A\beta_{40}$ (blue) and $RM_{CO520}A\beta_{42/40}$ (red). The spectral assignments in bold type were specifically given for (a) E11, (b) K16, and (c) E22. For brevity, brief assignments were given for other peaks. The peak positions of the weak signals had been confirmed by other relay cross peaks. The contour levels of all spectra were set as described in Fig. 3.

### Fibrillar aggregates of $RM_{CO520}A\beta_{42/40}$

By incubating $RM_{CO520}A\beta_{42/40}$ in phosphate buffer, we obtained the corresponding fibrillar aggregates (Fig. S28†). The NMR spectra of the wet pellets of the fibril samples were largely dominated by a single set of signals, except the signals of CO and $C^{\alpha}$ of I32 (Fig. S29–S32 and Table S5†). The average FWHM was 2.3 ppm (Fig. S33†), which was substantially sharper than that of the lyophilized oligomeric aggregates. However, such reduction in FWHM for the hydrated fibril samples were not unexpected because of the conformational averaging effect. From the secondary chemical shifts and the backbone torsion angles estimated by TALOS-N (Fig. S34†), fibrillar $RM_{CO520}A\beta_{42/}$

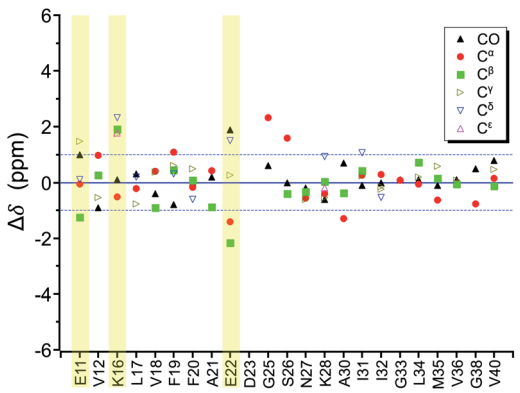


Fig. 7 Difference of chemical shifts (Δδ) between $RM_{CO520}A\beta_{42/40}$ and $RM_{CO520}A\beta_{40}$. The residues with the most notable chemical shift differences are highlighted with yellow bars. The two $C^{\gamma}$ signals of I32 were resolved.

$_{40}$ also exhibited the structural motif of $\beta_1$-loop-$\beta_2$ motif. While there were multiple weak signals of D23 for oligomeric $RM_{CO520}A\beta_{42/40}$, there was only one dominant set of D23 signals for fibrillar $RM_{CO520}A\beta_{42/40}$. The intensities of K16-$C^{\delta}/C^{\varepsilon}$, D23-$C^{\gamma}$/CO, and I32-$C^{\gamma}/C^{\beta}$ were stronger than those of the corresponding cross peaks of the oligomer spectra. By contrast, the cross peaks of E11-$C^{\delta}/C^{\alpha}$, E11-$C^{\delta}/C^{\gamma}$, V12-$C^{\gamma}/C^{\beta}$, F20-$C^{\beta}/C^{\delta}$, E22-$C^{\delta}/C^{\alpha}$, and V36-$C^{\beta}/C^{\alpha}$ of the fibril spectra were much weaker than those of the oligomer spectra. This remarkable observation revealed that the peptide conformation of $RM_{CO520}A\beta_{42/40}$ oligomers and fibrils might be similar, but their sidechain packings could be very different.

Fig. 8a shows the deviation between the chemical shift data of oligomeric and fibrillar $RM_{CO520}A\beta_{42/40}$. Interestingly, the top three largest deviations were again observed for the charged residues, *viz.*, E11, K16, and E22. We had envisioned two possible interpretations. First, the charged residues near the $\beta_1$ region of $A\beta_{40}$, together with D23, might play the key role in the structural rearrangement from high-MW oligomeric state to the fibrillar state. On the other hand, Fig. 8b illustrates that the chemical shift difference between $RM_{CO520}A\beta_{42/40}$ fibrils and $RM_{CO520}A\beta_{40}$ oligomers only exhibited a slightly larger root-mean-square deviation than the results shown in Fig. 7 and 8a. Thus, as an alternative interpretation, the chemical shift variation of these charged residues might merely reflect the fact that chemical shifts are sensitive to the charge state of these residues. Upon a change in intermolecular packing, the solvent exposure of the charged residues could have altered, leading to a variation of their electrostatic charges. However, this change in the chemical state is not necessarily accompanied with a major conformational change. This rationalization could also apply to the effect of $A\beta_{42}$Os on the aggregation of $A\beta_{40}$. An unequivocal interpretation of our chemical shift data may require the justifications by extensive theoretical calculations.

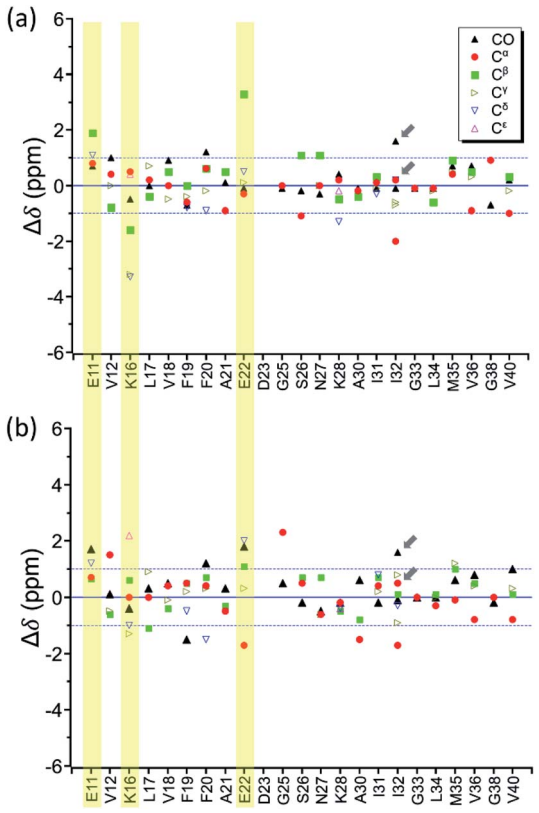


Fig. 8 Difference of chemical shifts ($\Delta\delta$) (a) between $RM_{CO520}A\beta_{42/40}$ fibrils and $RM_{CO520}A\beta_{42/40}$ oligomers; (b) between $RM_{CO520}A\beta_{42/40}$ fibrils and $RM_{CO520}A\beta_{40}$ oligomers. The residues with the most notable chemical shift differences in (a) are highlighted with yellow bars. The two $C^{\gamma}$ signals of I32 were resolved. The arrows indicate there were two sets of CO and $C^{\alpha}$ signals for I32.

# Discussion

### Use of reverse micelles as nano-incubator for amyloidogenic peptides

There are several different approaches developed to prepare high-MW AβOs.[84] All the methods reported thus far in the literature can be categorized as the passive approach, where the size distribution of the oligomers is primarily determined by the aggregation kinetics. In this work, we reported the use of RMs to prepare AβOs. A detailed discussion of the technical issues associated with the encapsulation of Aβ peptides within RMs is given in ESI.† The success of this protocol, as validated by the solid-state NMR data, has several important implications. First, it is well known that the toxicity of AβOs depends on its size.[8] Therefore, it is highly desirable to probe the structures of AβOs of different size. Because the chemistry of RMs is rather mature,[85] a judicious choice of surfactants and/or the oil phase can be used to control the size of reverse micelles, which in turn can allow an active control of the size of AβOs. To the best of our knowledge, such a control of the oligomeric state is not possible for other "passive" methods. Second, RM is an ideal device for the study of the protein–protein interactions associated with amyloidogenic peptides. On the one hand, the fusion and fission of RMs allow the material transfer among RMs. Thus, two different types of amyloidogenic peptides can be well mixed in RMs. On the other hand, the fusion-fission process has a tiny energy barrier.[57] Thus, the peptides encapsulated in a RM have significantly longer interaction time than in bulk solution. This may better mimic the crowded environment *in vivo*. On a more general note, the RM approach can be used as a platform to study protein–protein interactions for other amyloidogenic proteins such as α-synuclein, prion, TDP-43, tau, *etc.* Third, RMs could be used to amplify a minute quantity of the oligomeric species extracted from the brain tissues of AD patients, provided that the seeding kinetics are much faster than the homogeneous nucleation rate of the Aβ monomers. While the idea of seeding has been successfully adapted to amplify the fibrillar aggregates of brain extracts,[78] seeding in bulk solution cannot be used to amplify any oligomeric species because further transformation to mature fibrils cannot be avoided. Overall, our RM approach has provided an exciting possibility for a systematic study of oligomeric aggregates of amyloidogenic peptides and their more aggregation-prone mutants, prepared *in vitro* or derived from brain tissues.

### $A\beta_{40}$ aggregation seeded by $A\beta_{42}Os$

Aβ peptides can be found in many body fluids, such as cerebrospinal fluid, plasma, and brain. Under normal physiological conditions, $A\beta_{40}$ (80–90%) is more abundantly produced than $A\beta_{42}$ (5–10%).[86,87] For AD brains, however, $A\beta_{42}$ is the major component in the parenchymal plaques, whereas $A\beta_{40}$ is usually deposited in the cerebral vessels.[39,88] Many efforts have been dedicated to study the cross-seeding effect between them under *in vitro* conditions. In most of these studies the seeds were prepared by fragmentation of the mature fibrils. However, it is debatable whether it is biological relevant to study the interaction between the monomeric form of one Aβ form and the short fibril fragments of another form, because there is no *in vivo* evidence showing that the fibrillization of one Aβ form must precede another. Furthermore, it is very difficult to compare the cross-seeding data published by different laboratories if fibril-assisted secondary nucleation is an effective Aβ aggregation pathway. The notion of fibril-assisted nucleation is appealing because it can rationalize the observation that $A\beta_{42}$ fibrils can nucleate the fibrillogenesis of $A\beta_{40}$ but $A\beta_{42}$ protofibrils have no seeding effects on $A\beta_{40}$ monomers.[40] Thus, it is very likely that the aggregation kinetics depend on the surface structure of the fibrils, which is in turn strongly influenced by the incubation conditions.[89] Consequently, it may be a futile exercise to compare the vast body of literature in Aβ cross-seeding experiments because the molecular structure of the seeds were usually uncharacterized. In this work, we showed that high-MW $A\beta_{42}Os$ could seed the aggregation of $A\beta_{40}$ monomers. That is, both $A\beta_{40}Os$ and $A\beta_{42}Os$ could serve as "template" for the aggregation of $A\beta_{40}$ monomers. As a partial support to this conjecture, it has been reported that the spherical amyloid assembly (SPA) of $A\beta_{42}$ exhibited a β-loop-β motif,[76] similar to what we observed for $A\beta_{40}Os$. Altogether, our results suggest that the cross-seeding of Aβ *in vivo* does not necessarily require the formation of amyloid fibrils. Furthermore, the seeding effect of $A\beta_{42}Os$ on $A\beta_{40}$ might be dominated by electrostatic interactions *via* the charged residues. This inference is consistent with the observations that liposomes formed by charged lipids can accelerate the aggregation kinetics of Aβ.[90,91]

### On-pathway or off-pathway?

Recently, Hoyer and co-workers used a flexible $(Gly_4Ser)_4$ linker to covalently connect two $A\beta_{40}$ peptides in a head-to-tail fashion to form the so-called dimAβ molecules.[16] Surprisingly, the globular oligomeric aggregates of dimAβ, with an estimated size of 62 kDa,[92] would inhibit the nucleation and growth of Aβ fibrils. Consequently, the authors claimed that AβOs of sizes >50 kDa are not intermediates on the pathway to amyloid fibrils, *i.e.*, off-pathway.[16,92] While dimAβ may be considered as a reasonable mimic of two Aβ molecules in close proximity, it remains a single chimeric peptide. It is also unclear whether the same results would be obtained for the head-to-head or tail-to-tail fashions. Even though dimAβ can form fibrillar assembly, it does not imply that the oligomeric aggregates of dimAβ are structurally the same as AβOs. After all, neither the molecular structure of the oligomeric aggregates of dimAβ nor Aβ are known in the literature. The 3D reconstruction by cryoEM for the oligomeric aggregates of dimAβ had a spatial resolution of 17 Å only.[92] In this work, our seeding experiments provide a direct evidence that high-MW AβOs did not inhibit the fibrillization of $A\beta_{40}$ monomers. It remains an open question whether there is any structural similarity between the AβOs and the seeded fibrils. If they are structurally distinctive, the seeding phenomenon could be driven by non-specific molecular interactions. Thus, further investigation of the fibrillar structures of the seeded fibrils by cryoEM are warranted. In any case, the critical role of AβOs in AD pathogenesis is a consensus,[5,6,10–12,93,94] should it be on-pathway or off-pathway.

### Implications of the NMR data of $RM_{CO520}A\beta_{42/40}$

Although the solid-state NMR data unequivocally showed that $A\beta_{42}Os$ can modulate the peptide conformation of $A\beta_{40}Os$, it is not straightforward to unravel the underlying molecular events. While the chemical shift data of low-MW $A\beta_{40}Os$ and high-MW $A\beta_{40}Os$ are different,[23,26] it is well known that multiple distinct structures could be obtained for fibrils incubated under different conditions.[54] Yet, we cannot rule out the possibility that structural rearrangement could occur for $A\beta_{40}Os$ at different sizes. The NMR spectra of $RM_{CO520}A\beta_{40}$ and $RM_{CO520}A\beta_{42/40}$, which were of similar size and were incubated under the same conditions, might unravel the effects of $A\beta_{42}Os$ on the nucleation process of $A\beta_{40}Os$. As revealed in the chemical shift data, the residues of the $\beta_2$ region were less affected by the seeding effect. The significant perturbation of the $^{13}C$ chemical shifts of E11, K16, E22, G25, and S26 of $A\beta_{40}$ implies that their chemical states were altered during the nucleation process. The chemical shift perturbations at G25 and S26 seemed consistent with the observation that G25 and S26 of brain-derived $A\beta_{40}$ fibrils are solvent exposed.[78] However, the $^{13}C$ chemical shifts of CO and $C^{\beta}$ of S26 were almost the same for $RM_{CO520}A\beta_{42/40}$ and $RM_{CO520}A\beta_{40}$. Thus, the large deviation of $C^{\alpha}$ alone may not guarantee a major conformational change at S26. In addition, the hydrogen-sidechain of glycine should have very limited sidechain–sidechain interactions. Hence, we inferred that the sidechains of E11, K16, and E22 of $A\beta_{40}$ played an important role when its monomers aggregated on the surface of $A\beta_{42}Os$. This process should resemble the event of secondary nucleation. More experiments are required to verify whether or not other residues near the N-terminus were involved.

The central fragment of Aβ such as LVFF, KLVFF, KLVFFA, and KLVFFAE have been identified as the template for the development of Aβ inhibitors,[95–100] peptide homologs to attenuate fibril formation and moderately dissemble preformed fibrils,[101,102] and β-sheet-breaker peptides to reduce cerebral damage in APP transgenic mouse model.[103] Residues of F19 and F20 were considered to favor the nucleation of Aβ aggregation.[104] Mutations at residues of A21, E22, and D23 would affect the kinetics of nucleation in the fibrillization process of Aβ.[105] These studies reflect the consensus that the region of K16 to E22 is of great importance for Aβ aggregation. The solid-state NMR data for $RM_{CO520}A\beta_{42/40}$ shed additional insights into this widely accepted notion. Upon the interaction between $A\beta_{40}$

monomers and $A\beta_{42}$Os, there were chemical changes at K16 and E22. However, those residues in the hydrophobic region of LVFFA were not structurally altered as indicated by their relatively minor variation in chemical shifts. Yet, the presence of multiple peaks implies that this region might be susceptible to non-specific intermolecular interaction. The observation that E22 and K16 are involved in governing the interaction between $A\beta_{40}$ peptides and $A\beta_{42}$Os may look counterintuitive in the light of the genetics of familial AD, *viz.*, E22K (Italian), E22Q (Dutch), E22G (Arctic), and E22Δ (Osaka),[106] and the fact that the K16N mutation of APP produces highly toxic heteromeric Aβ oligomers.[107] However, we make no claim that electrostatic interactions are the only viable mechanism governing the interaction between $A\beta_{40}$ and $A\beta_{42}$. Thus, our results do not rule out the possibility that mutations at E22 might enhance the interactions between $A\beta_{40}$ and $A\beta_{42}$.

## Conclusions

The structure of AβOs prepared in bulk solution are intrinsically heterogeneous because AβOs are transient species and they would readily transform to fibrillar aggregates. We demonstrated that RMs could be exploited to provide an active control of the size of the AβOs. Our approach also opens a new avenue to study the interaction of monomer peptides with the oligomeric aggregates of other amyloidogenic peptides. This important advantage had been illustrated by our results that there were considerable differences for the chemical shifts of $A\beta_{40}$Os incubated with and without the influences of $A\beta_{42}$Os.

The cross-seeding effect of $A\beta_{42}$ aggregates on $A\beta_{40}$ is an important issue in Aβ research because it is a widespread notion that $A\beta_{42}$ could trigger amyloid plaque deposition. While early results on the cross-seeding effect are consistent with the notion, many recent studies argued that the fibrillar fragments of $A\beta_{42}$ have negligible seeding effect on $A\beta_{40}$. Herein, we reported that oligomeric aggregates of $A\beta_{42}$ could indeed accelerate the fibrillization process of $A\beta_{40}$. Our results indicated that a careful characterization of the aggregation state of the seeds is necessary to warrant a meaningful interpretation of any cross-seeding experiments. This may help resolve the controversy over the cross-seeding effect between $A\beta_{40}$ and $A\beta_{42}$.

## Data availability

All relevant data are presented in the main text and ESI.†

## Author contributions

J. C. C. C. designed the research, H. W. C., H. I. M., Y. S. W., and M. C. L. performed Aβ preparation and biophysical assays. E. C. Y. Y. and H. W. C. performed EA analysis and analyzed data. M. H. W., L. H. T., and M. C. L. prepared isotope-labeled Aβ peptide. H. W. C., H. I. M., and S. J. H. performed and analyzed ssNMR data. J. C. C. C. wrote the manuscript. All authors have given approval to the final version of the manuscript.

## Conflicts of interest

There are no conflicts to declare.

## Acknowledgements

This work was financially supported by the Ministry of Science and Technology (MOST 108-2113-M-002-001). The TMV samples were kindly provided by Dr Hsin-Hung Yeh and Dr Yi-Shu Chiu (Agricultural Biotechnological Research Center, Academia Sinica). The NMR, TEM, and STEM measurements were carried out at the Instrumentation Center of National Taiwan University, supported by the Ministry of Science and Technology. The assistance of Ya-Yun Yang in STEM measurements is gratefully acknowledged.

## Notes and references

1 J. A. Hardy and G. A. Higgins, *Science*, 1992, **256**, 184–185.
2 J. Hardy and D. J. Selkoe, *Science*, 2002, **297**, 353–356.
3 D. J. Selkoe and J. Hardy, *EMBO Mol. Med.*, 2016, **8**, 595–608.
4 C. Haass and D. J. Selkoe, *Nat. Rev. Mol. Cell Biol.*, 2007, **8**, 101–112.
5 D. M. Walsh and D. J. Selkoe, *J. Neurochem.*, 2007, **101**, 1172–1184.
6 K. L. Viola and W. L. Klein, *Acta Neuropathol.*, 2015, **129**, 183–206.
7 M. P. Lambert, A. K. Barlow, B. A. Chromy, C. Edwards, R. Freed, M. Liosatos, T. E. Morgan, I. Rozovsky, B. Trommer, K. L. Viola, P. Wals, C. Zhang, C. E. Finch, G. A. Krafft and W. L. Klein, *Proc. Natl. Acad. Sci.*, 1998, **95**, 6448–6453.
8 F. Bemporad and F. Chiti, *Chem. Biol.*, 2012, **19**, 315–327.
9 E. Y. Hayden and D. B. Teplow, *Alzheimer's Res. Ther.*, 2013, **5**, 60.
10 S. T. Ferreira, M. V. Lourenco, M. M. Oliveira and F. G. De Felice, *Front. Cell. Neurosci.*, 2015, **9**, 191.
11 E. N. Cline, M. A. Bicca, K. L. Viola and W. L. Klein, *J. Alzheimers Dis.*, 2018, **64**, S567–S610.
12 I. Benilova, E. Karran and B. De Strooper, *Nat. Neurosci.*, 2012, **15**, 349–357.
13 T. Härd, *FEBS J.*, 2011, **278**, 3884–3892.
14 T. Yamaguchi, H. Yagi, Y. Goto, K. Matsuzaki and M. Hoshino, *Biochemistry*, 2010, **49**, 7100–7107.
15 B. O'Nuallain, D. B. Freir, A. J. Nicoll, E. Risse, N. Ferguson, C. E. Herron, J. Collinge and D. M. Walsh, *J. Neurosci.*, 2010, **30**, 14411–14419.
16 F. Hasecke, T. Miti, C. Perez, J. Barton, D. Schölzel, L. Gremer, C. S. R. Grüning, G. Matthews, G. Meisl, T. P. J. Knowles, D. Willbold, P. Neudecker, H. Heise, G. Ullah, W. Hoyer and M. Muschol, *Chem. Sci.*, 2018, **9**, 5937–5948.
17 G. Bitan, A. Lomakin and D. B. Teplow, *J. Biol. Chem.*, 2001, **276**, 35176–35184.
18 G. Bitan, M. D. Kirkitadze, A. Lomakin, S. S. Vollers, G. B. Benedek and D. B. Teplow, *Proc. Natl. Acad. Sci.*, 2003, **100**, 330–335.

19 D. B. Teplow, N. D. Lazo, G. Bitan, S. Bernstein, T. Wyttenbach, M. T. Bowers, A. Baumketner, J. E. Shea, B. Urbanc, L. Cruz, J. Borreguero and H. E. Stanley, *Acc. Chem. Res.*, 2006, **39**, 635–645.
20 M. Serra-Batiste, M. Ninot-Pedrosa, M. Bayoumi, M. Gairí, G. Maglia and N. Carulla, *Proc. Natl. Acad. Sci.*, 2016, **113**, 10866–10871.
21 S. Ciudad, E. Puig, T. Botzanowski, M. Meigooni, A. S. Arango, J. Do, M. Mayzel, M. Bayoumi, S. Chaignepain, G. Maglia, S. Cianferani, V. Orekhov, E. Tajkhorshid, B. Bardiaux and N. Carulla, *Nat. Commun.*, 2020, **11**, 3014.
22 S. Chimon and Y. Ishii, *J. Am. Chem. Soc.*, 2005, **127**, 13472–13473.
23 S. Chimon, M. A. Shaibat, C. R. Jones, D. C. Calero, B. Aizezi and Y. Ishii, *Nat. Struct. Mol. Biol.*, 2007, **14**, 1157–1164.
24 M. Ahmed, J. Davis, D. Aucoin, T. Sato, S. Ahuja, S. Aimoto, J. I. Elliott, W. E. Van Nostrand and S. O. Smith, *Nat. Struct. Mol. Biol.*, 2010, **17**, 561–568.
25 W. B. Stine, L. Jungbauer, C. Yu and M. J. LaDu, in *Alzheimer's Disease and Frontotemporal Dementia: Methods and Protocols*, ed. E. D. Roberson, Humana Press, Totowa, NJ, 2011, pp. 13–32.
26 B. Sarkar, V. S. Mithu, B. Chandra, A. Mandal, M. Chandrakesan, D. Bhowmik, P. K. Madhu and S. Maiti, *Angew. Chem., Int. Ed.*, 2014, **53**, 6888–6892.
27 S. Parthasarathy, M. Inoue, Y. Xiao, Y. Matsumura, Y. Nabeshima, M. Hoshi and Y. Ishii, *J. Am. Chem. Soc.*, 2015, **137**, 6480–6483.
28 A. Potapov, W.-M. Yau, R. Ghirlando, K. R. Thurber and R. Tycko, *J. Am. Chem. Soc.*, 2015, **137**, 8294–8307.
29 Y. Miller, B. Ma and R. Nussinov, *Proc. Natl. Acad. Sci. U. S. A.*, 2010, **107**, 9490–9495.
30 T. M. Ryan, N. Kirby, H. D. T. Mertens, B. Roberts, K. J. Barnham, R. Cappai, C. L. L. Pham, C. L. Masters and C. C. Curtain, *Metallomics*, 2015, **7**, 536–543.
31 H. A. Scheidt, I. Morgado and D. Huster, *J. Biol. Chem.*, 2012, **287**, 22822–22826.
32 J. M. Lopez del Amo, U. Fink, M. Dasari, G. Grelle, E. E. Wanker, J. Bieschke and B. Reif, *J. Mol. Biol.*, 2012, **421**, 517–524.
33 J. Wang, T. Yamamoto, J. Bai, S. J. Cox, K. J. Korshavn, M. Monette and A. Ramamoorthy, *Chem. Commun.*, 2018, **54**, 2000–2003.
34 B. R. Sahoo, T. Genjo, M. Bekier, S. J. Cox, A. K. Stoddard, M. Ivanova, K. Yasuhara, C. A. Fierke, Y. Wang and A. Ramamoorthy, *Chem. Commun.*, 2018, **54**, 12883–12886.
35 T. Yang, S. Li, H. Xu, D. M. Walsh and D. J. Selkoe, *J. Neurosci.*, 2017, **37**, 152–163.
36 D. A. White, A. K. Buell, T. P. J. Knowles, M. E. Welland and C. M. Dobson, *J. Am. Chem. Soc.*, 2010, **132**, 5170–5175.
37 J. T. Jarrett and P. T. Lansbury, *Cell*, 1993, **73**, 1055–1058.
38 A. Lomakin, D. S. Chung, G. B. Benedek, D. A. Kirschner and D. B. Teplow, *Proc. Natl. Acad. Sci. U. S. A.*, 1996, **93**, 1125–1129.
39 J. T. Jarrett, E. P. Berger and P. T. Lansbury, *Biochemistry*, 1993, **32**, 4693–4697.
40 A. Jan, O. Gokce, R. Luthi-Carter and H. A. Lashuel, *J. Biol. Chem.*, 2008, **283**, 28176–28189.
41 K. Hasegawa, I. Yamaguchi, S. Omata, F. Gejyo and H. Naiki, *Biochemistry*, 1999, **38**, 15514–15521.
42 S. W. Snyder, U. S. Ladror, W. S. Wade, G. T. Wang, L. W. Barrett, E. D. Matayoshi, H. J. Huffaker, G. A. Krafft and T. F. Holzman, *Biophys. J.*, 1994, **67**, 1216–1228.
43 K. Ono, R. Takahashi, T. Ikeda and M. Yamada, *J. Neurochem.*, 2012, **122**, 883–890.
44 D. Frost, P. M. Gorman, C. M. Yip and A. Chakrabartty, *Eur. J. Biochem.*, 2003, **270**, 654–663.
45 R. Cukalevski, X. Yang, G. Meisl, U. Weininger, K. Bernfur, B. Frohm, T. P. J. Knowles and S. Linse, *Chem. Sci.*, 2015, **6**, 4215–4233.
46 B. K. Yoo, Y. Xiao, D. McElheny and Y. Ishii, *J. Am. Chem. Soc.*, 2018, **140**, 2781–2784.
47 Y. Xiao, B. Ma, D. McElheny, S. Parthasarathy, F. Long, M. Hoshi, R. Nussinov and Y. Ishii, *Nat. Struct. Mol. Biol.*, 2015, **22**, 499–505.
48 M. T. Colvin, R. Silvers, Q. Z. Ni, T. V. Can, I. Sergeyev, M. Rosay, K. J. Donovan, B. Michael, J. Wall, S. Linse and R. G. Griffin, *J. Am. Chem. Soc.*, 2016, **138**, 9663–9674.
49 M. A. Wälti, F. Ravotti, H. Arai, C. G. Glabe, J. S. Wall, A. Böckmann, P. Güntert, B. H. Meier and R. Riek, *Proc. Natl. Acad. Sci.*, 2016, **113**, E4976–E4984.
50 S. I. A. Cohen, S. Linse, L. M. Luheshi, E. Hellstrand, D. A. White, L. Rajah, D. E. Otzen, M. Vendruscolo, C. M. Dobson and T. P. J. Knowles, *Proc. Natl. Acad. Sci.*, 2013, **110**, 9758–9763.
51 G. A. Garcia, S. I. A. Cohen, C. M. Dobson and T. P. J. Knowles, *Phys. Rev. E: Stat., Nonlinear, Soft Matter Phys.*, 2014, **89**, 032712.
52 T. P. J. Knowles, M. Vendruscolo and C. M. Dobson, *Nat. Rev. Mol. Cell Biol.*, 2014, **15**, 384–396.
53 G. Meisl, X. Yang, E. Hellstrand, B. Frohm, J. B. Kirkegaard, S. I. A. Cohen, C. M. Dobson, S. Linse and T. P. J. Knowles, *Proc. Natl. Acad. Sci. U. S. A.*, 2014, **111**, 9384–9389.
54 R. Tycko, *Neuron*, 2015, **86**, 632–645.
55 P. L. Luisi, M. Giomini, M. P. Pileni and B. H. Robinson, *Biochim. Biophys. Acta, Biomembr.*, 1988, **947**, 209–246.
56 M. P. Pileni, *J. Phys. Chem.*, 1993, **97**, 6961–6973.
57 P. D. I. Fletcher, A. M. Howe and B. H. Robinson, *J. Chem. Soc., Faraday Trans. 1*, 1987, **83**, 985–1006.
58 E. Ruckenstein and P. Karpe, *J. Phys. Chem.*, 1991, **95**, 4869–4882.
59 Y. Miyake, *Colloids Surf., A*, 1996, **109**, 255–262.
60 Y.-L. Lin, Y.-S. Cheng, C.-I. Ho, Z.-H. Guo, S.-J. Huang, M.-L. Org, A. Oss, A. Samoson and J. C. C. Chan, *Chem. Commun.*, 2018, **54**, 10459–10462.
61 J.-L. Lemyre, S. Lamarre, A. Beaupré and A. M. Ritcey, *Langmuir*, 2010, **26**, 10524–10531.
62 M.-C. Lee, W.-C. Yu, Y.-H. Shih, C.-Y. Chen, Z.-H. Guo, S.-J. Huang, J. C. C. Chan and Y.-R. Chen, *Sci. Rep.*, 2018, **8**, 4772.
63 B. Chen, K. R. Thurber, F. Shewmaker, R. B. Wickner and R. Tycko, *Proc. Natl. Acad. Sci. U. S. A.*, 2009, **106**, 14339–14344.

64 M. Hoshi, M. Sato, S. Matsumoto, A. Noguchi, K. Yasutake, N. Yoshida and K. Sato, *Proc. Natl. Acad. Sci.*, 2003, **100**, 6370–6375.
65 A. Noguchi, S. Matsumura, M. Dezawa, M. Tada, M. Yanazawa, A. Ito, M. Akioka, S. Kikuchi, M. Sato, S. Ideno, M. Noda, A. Fukunari, S. Muramatsu, Y. Itokazu, K. Sato, H. Takahashi, D. B. Teplow, Y. Nabeshima, A. Kakita, K. Imahori and M. Hoshi, *J. Biol. Chem.*, 2009, **284**, 32895–32905.
66 R. W. Hepler, K. M. Grimm, D. D. Nahas, R. Breese, E. C. Dodson, P. Acton, P. M. Keller, M. Yeager, H. Wang, P. Shughrue, G. Kinney and J. G. Joyce, *Biochemistry*, 2006, **45**, 15157–15167.
67 W. Yong, A. Lomakin, M. D. Kirkitadze, D. B. Teplow, S.-H. Chen and G. B. Benedek, *Proc. Natl. Acad. Sci.*, 2002, **99**, 150–154.
68 R. Sabaté and J. Estelrich, *J. Phys. Chem. B*, 2005, **109**, 11027–11032.
69 J. Tran, D. Chang, F. Hsu, H. Wang and Z. Guo, *FEBS Lett.*, 2017, **591**, 177–185.
70 M. So, A. Ishii, Y. Hata, H. Yagi, H. Naiki and Y. Goto, *Langmuir*, 2015, **31**, 9973–9982.
71 G. A. Braun, A. J. Dear, K. Sanagavarapu, H. Zetterberg and S. Linse, *Chem. Sci.*, 2022, **13**, 2423–2439.
72 Y. Yan and C. Wang, *J. Mol. Biol.*, 2007, **369**, 909–916.
73 T. Yamaguchi, K. Matsuzaki and M. Hoshino, *FEBS Lett.*, 2013, **587**, 620–624.
74 A. T. Petkova, Y. Ishii, J. J. Balbach, O. N. Antzutkin, R. D. Leapman, F. Delaglio and R. Tycko, *Proc. Natl. Acad. Sci.*, 2002, **99**, 16742–16747.
75 Y. Shen and A. Bax, in *Artificial Neural Networks*, ed. H. Cartwright, Springer, New York, NY, 2015, pp. 17–32.
76 Y. Xiao, I. Matsuda, M. Inoue, T. Sasahara, M. Hohi, s and Y. Ishii, *J. Biol. Chem.*, 2020, **295**, 458–467.
77 A. T. Petkova, R. D. Leapman, Z. H. Guo, W. M. Yau, M. P. Mattson and R. Tycko, *Science*, 2005, **307**, 262–265.
78 J.-X. Lu, W. Qiang, W.-M. Yau, C. D. Schwieters, S. C. Meredith and R. Tycko, *Cell*, 2013, **154**, 1257–1268.
79 W. Qiang, W.-M. Yau, J.-X. Lu, J. Collinge and R. Tycko, *Nature*, 2017, **541**, 217–221.
80 U. Ghosh, K. R. Thurber, W.-M. Yau and R. Tycko, *Proc. Natl. Acad. Sci.*, 2021, **118**, e2023089118.
81 A. Daskalov, M. Gantner, M. A. Wälti, T. Schmidlin, C. N. Chi, C. Wasmer, A. Schütz, J. Ceschin, C. Clavé, S. Cescau, B. Meier, R. Riek and S. J. Saupe, *PLoS Pathog.*, 2014, **10**, e1004158.
82 J. C. Stroud, C. Liu, P. K. Teng and D. Eisenberg, *Proc. Natl. Acad. Sci.*, 2012, **109**, 7717–7722.
83 M. Kollmer, W. Close, L. Funk, J. Rasmussen, A. Bsoul, A. Schierhorn, M. Schmidt, C. J. Sigurdson, M. Jucker and M. Fändrich, *Nat. Commun.*, 2019, **10**, 1–8.
84 B. R. Sahoo, S. J. Cox and A. Ramamoorthy, *Chem. Commun.*, 2020, **56**, 4627–4639.
85 J. Eastoe, M. J. Hollamby and L. Hudson, *Adv. Colloid Interface Sci.*, 2006, **128–130**, 5–15.
86 D. J. Selkoe, *Physiol. Rev.*, 2001, **81**, 741–766.
87 M. P. Murphy and H. LeVine, *J. Alzheimer's Dis.*, 2010, **19**, 311–323.
88 A. Charidimou, G. Boulouis, M. E. Gurol, C. Ayata, B. J. Bacskai, M. P. Frosch, A. Viswanathan and S. M. Greenberg, *Brain*, 2017, **140**, 1829–1850.
89 A. K. Paravastu, R. D. Leapman, W. M. Yau and R. Tycko, *Proc. Natl. Acad. Sci. U. S. A.*, 2008, **105**, 18349–18354.
90 M. Bokvist, F. Lindström, A. Watts and G. Gröbner, *J. Mol. Biol.*, 2004, **335**, 1039–1049.
91 K. Matsuzaki, *Biochim. Biophys. Acta, Biomembr.*, 2007, **1768**, 1935–1942.
92 M. P. Schützmann, F. Hasecke, S. Bachmann, M. Zielinski, S. Hänsch, G. F. Schröder, H. Zempel and W. Hoyer, *Nat. Commun.*, 2021, **12**, 4634.
93 W. M. Berhanu and U. H. E. Hansmann, *Adv. Protein Chem. Struct. Biol.*, 2014, **96**, 113–141.
94 L. Nagel-Steger, M. C. Owen and B. Strodel, *ChemBioChem*, 2016, **17**, 657–676.
95 L. O. Tjernberg, J. Näslund, F. Lindqvist, J. Johansson, A. R. Karlström, J. Thyberg, L. Terenius and C. Nordstedt, *J. Biol. Chem.*, 1996, **271**, 8545–8548.
96 M. A. Findeis, G. M. Musso, C. C. Arico-Muendel, H. W. Benjamin, A. M. Hundal, J.-J. Lee, J. Chin, M. Kelley, J. Wakefield, N. J. Hayward and S. M. Molineaux, *Biochemistry*, 1999, **38**, 6791–6800.
97 D. J. Gordon, K. L. Sciarretta and S. C. Meredith, *Biochemistry*, 2001, **40**, 8237–8245.
98 R. J. Chalifour, R. W. McLaughlin, L. Lavoie, C. Morissette, N. Tremblay, M. Boulé, P. Sarazin, D. Stéa, D. Lacombe, P. Tremblay and F. Gervais, *J. Biol. Chem.*, 2003, **278**, 34874–34881.
99 T. Takahashi and H. Mihara, *Acc. Chem. Res.*, 2008, **41**, 1309–1318.
100 M. Ouberai, P. Dumy, S. Chierici and J. Garcia, *Bioconjugate Chem.*, 2009, **20**, 2123–2132.
101 C. Soto, M. S. Kindy, M. Baumann and B. Frangione, *Biochem. Biophys. Res. Commun.*, 1996, **226**, 672–680.
102 M. A. Chacón, M. I. Barría, C. Soto and N. C. Inestrosa, *Mol. Psychiatry*, 2004, **9**, 953–961.
103 B. Permanne, C. Adessi, G. P. Saborio, S. Fraga, M.-J. Frossard, J. V. Dorpe, I. Dewachter, W. A. Banks, F. V. Leuven and C. Soto, *FASEB J.*, 2002, **16**, 860–862.
104 R. Cukalevski, B. Boland, B. Frohm, E. Thulin, D. Walsh and S. Linse, *ACS Chem. Neurosci.*, 2012, **3**, 1008–1016.
105 C.-L. Ni, H.-P. Shi, H.-M. Yu, Y.-C. Chang and Y.-R. Chen, *FASEB J.*, 2011, **25**, 1390–1401.
106 J. Nasica-Labouze, P. H. Nguyen, F. Sterpone, O. Berthoumieu, N.-V. Buchete, S. Coté, A. De Simone, A. J. Doig, P. Faller, A. Garcia, A. Laio, M. S. Li, S. Melchionna, N. Mousseau, Y. Mu, A. Paravastu, S. Pasquali, D. J. Rosenman, B. Strodel, B. Tarus, J. H. Viles, T. Zhang, C. Wang and P. Derreumaux, *Chem. Rev.*, 2015, **115**, 3518–3563.
107 D. Kaden, A. Harmeier, C. Weise, L. M. Munter, V. Althoff, B. R. Rost, P. W. Hildebrand, D. Schmitz, M. Schaefer, R. Lurz, S. Skodda, R. Yamamoto, S. Arlt, U. Finckh and G. Multhaup, *EMBO Mol. Med.*, 2012, **4**, 647–659.